Since January 2020 Elsevier has created a COVID-19 resource centre with free information in English and Mandarin on the novel coronavirus COVID-19. The COVID-19 resource centre is hosted on Elsevier Connect, the company's public news and information website.

Computers, Environment and Urban Systems 83 (2020) 101520

Contents lists available at ScienceDirect

Computers, Environment and Urban Systems

journal homepage: www.elsevier.com/locate/ceus

Impact of extreme weather events on urban human flow: A perspective from location-based service data

Zhenhua Chen[a,*], Zhaoya Gong[b,*], Shan Yang[a], Qiwei Ma[c], Changcheng Kan[d]

[a] City and Regional Planning, The Ohio State University, Columbus, OH, USA
[b] School of Geography, Earth and Environmental Sciences, University of Birmingham, Birmingham, UK
[c] School of Architecture, Tsinghua University, Beijing, China
[d] Baidu Online Network Technology (Beijing) Co., Ltd, Beijing, China

ARTICLE INFO

Keywords:
Disaster analysis
Urban human flow
Location-based service data
AMOEBA
Baidu map

ABSTRACT

This study investigates the impact of extreme weather events on urban human flow disruptions using location-based service data obtained from Baidu Map. Utilizing the 2018 Typhoon Mangkhut as an example, the spatial and temporal variations of urban human flow patterns in Shenzhen are examined using GIS and spatial flow analysis. In addition, the variation of human flow by different urban functions (e.g. transport, recreational, institutional, commercial and residential related facilities) is also examined through an integration of flow data and point-of-interest (POI) data. The study reveals that urban flow patterns varied substantially before, during, and after the typhoon. Specifically, urban flows were found to have reduced by 39% during the disruption. Conversely, 56% of flows increased immediately after the disruption. In terms of functional variation, the assessment reveals that fundamental urban functions, such as industrial (work) and institutional - (education) related trips experienced less disruption, whereas the typhoon event appears to have a relatively larger negative influence on recreational related trips. Overall, the study provides implications for planners and policy makers to enhance urban resilience to disasters through a better understanding of the urban vulnerability to disruptive events.

1. Introduction

Cities have experienced a rising number of disruptions from various types of unexpected weather events due to changes in climate and the environment. The occurrence of extreme weather events such as snowstorms, typhoons, and large rainstorms has not only caused damages on properties and urban infrastructure systems, human activities can also be severely affected. For instance, human mobility is significantly affected by the shutdown of major airports and railway stations. Urban activities such as tourism and sporting events can also be severely affected or cancelled in order to avoid further negative consequences. In addition, extreme weather events may lead to power outages or damage to infrastructure, which may further exacerbate the disruptions of urban functions and human activities. In fact, the damages caused by natural disasters to human society have increased substantially over the past six decades (Berke, 1995; Mileti, 1999; Dewan, 2013). In particular, the frequency and severity of hurricanes and typhoons has increased substantially, which has caused major damage to numerous cities along coastal areas in Asia-Pacific regions (Smith & Katz 2013). As a result, it has become a key challenge for urban planners handling emergency response and management to understand the impact of extreme weather events on human activities, in order to allow for the development of smart, resilient, and sustainable cities. Although an increasing number of studies have attempted to quantify the impacts of extreme weather events on the damages of physical infrastructure systems, such as transportation, energy, and water supplies, it remains unclear to what extent urban human activities are affected. One of the major challenges is due to the limitation of data. For instance, the traditional data source is often household surveys. Despite the advantage of revealing detailed behavioral changes in human activities before and after the occurrence of a disruptive event, such data also have limitations. For instance, the cost of data collection is very high and sample sizes are generally considerably small. In addition, the data is often collected in an ad hoc manner (e.g. collected during a specific time period and/or with a specific geographic focus). As a result, the dynamic spatiotemporal evolution of human activities due to the influence of extreme weather events can hardly be captured.

Conversely, the wide adoption of information and communications

* Corresponding authors.
E-mail addresses: chen.7172@osu.edu (Z. Chen), z.gong@bham.ac.uk (Z. Gong).

https://doi.org/10.1016/j.compenvurbsys.2020.101520
Received 12 November 2019; Received in revised form 28 February 2020; Accepted 25 June 2020
Available online 07 July 2020

technology (ICT), such as GPS-based sensors and smart phones, has facilitated the sharing and application of geospatial information considerably. In addition, a large volume of data are also generated from location-based services (LBS) at an unprecedented pace in terms of velocity, variety, and veracity through various types of social mobile apps, such as Twitter, WeChat, and Google apps. Although such data have provided new opportunities for urban analysts and planners to examine human dynamics, particularly in the context of disaster response and management (Shaw et al., 2016), there is still a lack of understanding in terms of how such data can be effectively adopted to address key issues related to urban disaster response and management.

To fill this research gap, this study provides an empirical assessment of the impact of extreme weather event on urban human flows. Using human mobility data collected by Baidu Maps, one of the biggest LBS providers in China, our study contributes to the field of geospatial big data analytics for smart cities in the following aspects:

Firstly, our study provides an in-depth assessment of the impact of extreme weather events on urban human flow changes through capturing dynamic evolutional patterns over time. Using Typhoon Mangkhut in Shenzhen as an example, for the first time the daily dynamics of human mobility and the impact of the disruption at a fine spatial scale (500 m × 500 m) were analyzed from the period of September 11–23, 2018 that covers the days before, during, and after the storm.

Secondly, the spatial and functional variations in human mobility flows were examined over time using both classic GIS methods and spatial flow analysis. A novel measure for comparing the spatial flow patterns over time was developed to quantify the temporal change in spatial flow structures and assess the impact of disruptions on urban flow. Through a combination of flow data with point-of-interest data, our analysis provides a detailed assessment of flow volume changes by different categories of urban functions (including commercial, industrial, institutional, recreational, residential, and transport). The assessment of urban flow variations among different urban functions enables planners to understand the impact of disruptive events on various types of human activities, which may provide evidence for land use planning and identify social and economic impacts from a new angle.

Thirdly, the analytical framework provides implications for urban vulnerability and resilience assessments under various unexpected events using location-based big data. In addition, the application introduced in this paper also has the potential to be utilized in the planning practice, given that such an analysis may help emergency management agencies identify vulnerable locations and time periods in consideration of human flow quantitatively. This could allow resources to be allocated more effectively in order to avoid or reduce the damage from a given disruptive event.

The rest of the paper is organized as follows. Section 2 identifies the research gaps through a comprehensive review of relevant literature. Sections 3 and 4 present the data and methodology, respectively. Section 5 discusses the analytical results, whereas section 6 summarizes and concludes.

2. Literature review

Location-based service (LBS) data has been extensive applied to study human flow patterns in recent years. Compared to traditional survey data, this new form can be collected much more easily (Chen and Schintler, 2015). The data also includes useful information such as flow trajectories with a spatial-temporal dimension (Brockmann et al., 2006, Gonzalez et al., 2008, Liang et al., 2012, Lee and Holme, 2015, Calabrese et al., 2010, Oliveira et al., 2016, Rhee et al., 2011, Xu et al., 2019, Papandrea et al., 2016, Yuan et al., 2012, Wang et al., 2017). The most common adoption of LBS data is to understand the spatial distribution patterns of human mobility. For instance, based on the analysis of call detail records (CDRs) of anonymized mobile phone users, Gonzalez et al. (2008) revealed that the power law distribution reflects the patterns of individual mobility in normal conditions. Conversely, through an assessment of the location-based data of bank notes, Brockmann et al. (2006) found that human mobility follows a power-law with a heavy-tailed distribution. In addition, based on an analysis of more than 20 million taxi trajectories in Beijing, Liang et al. (2012) revealed that the movement of taxis in normal conditions followed an exponential distribution instead of a power-law; in other words, they suggested that the displacement of taxis decays exponentially in an urban environment. Similarly, Yuan et al. (2012) examined the regional functions of Beijing utilizing similar datasets. Their study found that the pattern is very similar to land-use maps and they indicated that such data enables us to understand the distributional patterns of Points of Interest (POIs) and the intensity of human mobility in urban environments.

LBS data has also been adopted to understand the linkages between land use and human mobility patterns. For instance, Lee and Holme (2015) showed that mobility could be predicted through a combination of land-use maps and Origin-Destination (OD) survey data, given the fact that a strong linkage between land use and human mobility was identified. Similarly, Calabrese et al. (2010) predicted individual's locations based on both individual and collective behaviors using land use maps and a dataset of mobile phone locations in the Boston metropolitan area. The land use maps were classified using POIs data. In addition, Oliveira et al. (2016) investigated the locations of GPS users and its associated coverage time at given POIs using various data sources, including CDRs, GeoLife data, and OpenStreetMap data. Their study revealed that human mobility has a similar regularity and tends to be confined to certain areas among different cities. The movement of individuals was also analyzed by Papandrea et al. (2016) using both POI data and CDR data. Their study showed that an individual's mobility is primarily determined by the locations of their home and workplace. In general, the majority of human flows were found to be less than 10 km in urban areas. Such a pattern possesses similar statistical features to Levy walk, which is characterized by the distribution of heavy-tail flight and pause-time (Rhee et al., 2011).

Although many studies have attempted to examine the patterns of human mobility in normal conditions using LBS data, there is still a limited understanding of to what extent the patterns of urban human flow may differ under unexpected events, such as man-made disruptions (e.g. strikes and protests), natural disasters, and technological system failures. Among a few exceptions, Ahmouda et al. (2019) suggest that power-law models within the Lévy walk distributional pattern provide an effective applicability to examine human mobility patterns, both in normal and abnormal conditions. Similarly, Wang and Taylor (2016) also confirmed that individual mobility follows the power-law distribution (Levy flight model) in most disaster cases.

In terms of the application of different types of LBS data, Table 1 summarizes a few relevant studies based on LBS data for human flow-related disaster analysis. Specifically, three types of LBS data are commonly adopted to investigate the patterns of human mobility in disaster scenarios. The first one is geotagged social media data. For instance, geotagged Twitter data has been extensively adopted to examine how human mobility is affected by hurricanes (Ahmouda et al., 2019; Martín et al., 2017; Roy et al., 2019; Wang and Taylor, 2014). Some studies, such as Han et al. (2019) and Yabe et al. (2019a), examined this issue with a particular focus on evacuation and returning behaviors after disasters. Spatial statistical analysis and spatiotemporal comparative analysis are the most common approaches for their assessments.

The second most widely-adopted LBS data is mobile phone tower data, which is also known as cellular signaling data. The data, such as call detail records, is generated through the communication between cell phones and cellular tower stations. These data have also been frequently adopted to estimate human mobility and evacuation behaviors before disasters (Bengtsson et al., 2011; Khaefi et al., 2018, Lu et al.,

Table 1
Summary of the relevant studies using different data for disaster related human mobility analysis.

Author	Hazard type	Research question	Data type	Method
Ahmouda et al. (2019)	Hurricane	How do hurricanes affect human mobility (trip distance, radius of gyration, and mean square)?	Social media: geotagged Twitter data	Spatial statistical analysis
Bengtsson et al. (2011)	Earthquake	How can we estimate human mobility in a disaster using mobile phone data?	Mobile phone data from SIM cards: mobile phone tower data	Spatiotemporal estimation and comparison
Han et al. (2019)	Hurricane	How can Twitter data be used to understand spatiotemporal mobility patterns of evacuation zone residents during hurricane evacuation?	Social media: geotagged Twitter data	Spatiotemporal comparison using GIS, source list identification method (SLIM) for noise filtering
Joo et al. (2019)	Flood	What are the factors that influence people's evacuation behavior during a flood?	Mobile data from smartphone: Agoop location-based data	Spatial analysis using GIS and estimation using logistic regression
Khaefi et al. (2018)	Eruption	How can we predict evacuation destinations before a disaster happens by applying machine learning approaches to spatiotemporal data?	Antenna geolocation data and Mobile phone data from SIM cards: mobile phone tower data	Mobility prediction model using machine learning
Liu et al. (2019)	Typhoon	How can we use geo-tagged data to examine collective human activities during a typhoon?	Mobile data from smartphones: Tencent location-based data (https://heat.qq.com)	Spatiotemporal analysis with Multilevel Abrupt Changes Detection (MACD) framework
Martín et al. (2017)	Hurricane	How do we use geotagged data to establish spatiotemporal patterns of people's evacuation behaviors for hurricanes?	Social media: geotagged Twitter data	Spatiotemporal analysis using GIS
Roy et al. (2019)	Hurricane, earthquake, winter storm, etc.	How can we measure human mobility resilience to disasters using geotagged Twitter data?	Social media: geotagged Twitter data	Spatiotemporal analysis and comparative analysis
Song et al. (2014)	Earthquake	How can we understand and predict human mobility during earthquake evacuations using GPS records from mobile phones?	Mobile phone data: auto-GPS mobile sensor data	Probabilistic model using a machine learning framework
Yabe et al. (2019a)	Hurricane	How can we predict the returning behavior of evacuees after severe disasters?	Social media: geotagged Twitter data	Spatiotemporal analysis using machine learning
Yabe et al. (2019b)	Earthquake	To what extent the evacuation behavior is affected by earthquakes?	Mobile data from smartphones: Yahoo Japan Corporation	Spatial analysis and cross-comparative analysis

Source: Authors' summary.

2012). In terms of research methods, while spatiotemporal estimations and comparisons have generally been used, new methods such as machine learning have also been adopted for the prediction of mobility patterns using this type of data.

The third one is location-based service data, or mobile data collected from smartphones. The data can be collected based on either GPS, Wi-Fi signals, or cellular signals. Various types of LBS data have been adopted for disaster related human mobility analysis. For instance, Joo et al. (2019) studied the factors that affect evacuation behaviors during floods using one of the major types of LBS data, based in Japan, called Agoop. Similarly, Yabe et al. (2019b) investigated evacuation behaviors after earthquakes using the LBS data of Yahoo in Japan. Their study revealed that the probability of an individual's evacuation is strongly dependent on the seismic intensity they experience. Another LBS data called Tencent was applied to examine the collective human activities during typhoons in China. Their study revealed that there are significant spatial differences in the recovery duration of human activities after typhoons.

In sum, although a rising number of studies have attempted to reveal human mobility patterns both in normal conditions and disaster scenarios, the understanding of how urban human flow varies temporally and spatially (e.g. by different spatial clusters) in extreme weather events remains limited. In addition, it remains unclear to what extent human flow may vary among different urban functions, manifested by land use patterns of origins and destinations. It is also unclear how LBS data can be utilized to evaluate the vulnerability and resilience of urban systems to various unexpected circumstances, such as extreme weather events.[1]

Hence, this study fills these research gaps with a focus on addressing the following research questions: to what extent are urban human activities disrupted under extreme weather conditions? How does urban human flow vary spatially and functionally as a response to extreme weather conditions over time? And finally, what are the implications of LBS data for urban risk management and resilience capacity development?

3. Data and study area

3.1. Typhoon Mangkhut

Typhoon Mangkhut was one of the major disruptive weather events and a category 5 super typhoon occurred in 2018. It is one of the most powerful tropical cyclones ever recorded in the Asian-Pacific region and caused widespread damage among several Southeast Asian countries and regions such as Guam, the Philippines, Malaysia, Vietnam, and South China. Typhoon Mangkhut formed on September 6, 2018 over the Pacific Ocean and its magnitude and power grew as it moved towards Southeast Asia. It approached closest to South China on September 15, 2018. The meteorological bureaus of most cities in Guangdong province in China issued red alerts, which are the highest level, for Typhoon Mangkhu. Specifically, the Meteorological Bureau of Shenzhen issued a red alert for rainstorms on September 16, 2018.

The occurrence of Typhoon Mangkhut also caused massive disruptions of urban human activities. For instance, it is reported that over 2.45 million people were relocated in Guangdong province (Liang, 2018). The storm also caused a series of damages to the urban infrastructure system in Shenzhen. For instance, power failures occurred in over 13 location, many streets flooded, and over 248 trees were uprooted, which also caused disruptions to urban roadway systems (Han, 2018).

3.2. Data for the analysis

To provide a comprehensive assessment of the spatiotemporal variation of urban human flow in the city during the typhoon, three types of data were adopted in our assessment:

Urban flow data: The daily flow data for the study period were obtained from mobile device positioning by Baidu Maps, one of the largest location-based service providers in China (similar to Google Maps). For instance, the LBS platform of Baidu Maps holds the largest share (52.98%) of the LBS market in China (Li, 2018) and has more than 400 million monthly active user devices on average. Hence, these data provide a much broader representation of urban human mobility than other types of LBS data. The dataset includes more than 89 million flows among the location cell in Shenzhen. Each location is defined as a grid of 500 m × 500 m cell, which is a relatively high spatial resolution at which this type of data can be provided due to the concern of data privacy. Each flow record includes two types of information: the geospatial information of the centroids of its associated origin and destination (OD) cells, and the number of trips made by mobile device users moving from one origin to a different destination within one day. Therefore, trips made within the same grid are not included. Such an assumption is reasonable as the analysis was conducted based on the data with a relative high spatial resolution. As the flow volume is measured by count, the dataset does not differentiate individual users, as it can reflect multiple trips made by one user in a single day.

The data covers the period of September 10–23, 2018 (14 days). It includes seven days before the severe disruption of Typhoon Mangkhut (9.10–9.15), two days during the event (9.16–9.17) and five days after (9.18–9.23). The definition of the typhoon-affected period was based on typhoon alerts from the Meteorological Bureau of Shenzhen.

Point-of-interest (POI) data: Over 840,000 of POI data in Shenzhen was also obtained from Baidu Maps. The data include detailed spatial information of each POI. As shown in Table 2, POI is classified as 19 categories of urban functions.

Population density: The data is generated based on user check-ins on Baidu Maps. It can be used to reflect the vitality of different districts in a city. The data is primarily used for visualization to understand the spatial distribution of human activities in cities.

3.3. Study area

Shenzhen, with a total area of 1992 km^2, is one of the major subprovincial cities in Guangdong Province in China. The city locates in the core of the Guangdong – Hong Kong and Macau Great Bay Area and it is considered one of the most vibrant cities in China due to its fast-growing economy and well-developed high-tech sectors. While the cities attract millions of visitors and people every year, the city also suffers from tropical storms and typhoons during summer seasons.

The temporal distribution of urban flows is summarized in Fig. 1. The average daily flow volume is around 6.4 million. However, it is quite clear that during the two days of disruption from Typhoon Mangkhut, the volume of urban flows decreased substantially.

Fig. 2 summarizes the spatial distributions of urban human activities based on various LBS data. The figure in general depicts a polycentric urban structure in Shenzhen (Liu et al., 2018). Specifically, Fig. 2(a) and (b) reveal the distribution of population density in Shenzhen. It is clear that the central (Luohu, Futian, and Longhua) and western (Nanshan and Bao'an) regions have relatively higher levels of human activity, whereas the levels are generally lower in the rest of the city. Such a spatial pattern is also confirmed in Fig. 2(c), which is based on POI data. In addition, Fig. 2(c) also reveals that while commercial facilities cover mostly areas with high density, industrial facilitates are generally located in the north side of the city. In addition, to provide a

[1] Vulnerability is generally defined as the susceptibility to perturbations, which focuses on the consequence component of risk (Taylor, 2017). Conversely, resilience is a concept that reflects an ability of the economic and social system to maintain its function and/or hasten the speed of recovery after a shock from a disaster (Rose, 2004).

Table 2
Classification of land function.

Function of land	Secondary classification of POIs
Residential	Residential area, dormitory
Commercial	Restaurant, snack bar, cake dessert shop, cafe, bar, star hotel, express hotel, apartment hotel, shopping center, department store, supermarket, convenience store, home building material, home appliances digital, shop, market, communication business hall, post office, logistics company, ticket office, laundry, graphic fast printing shop, photo studio, real estate agency, public utility, maintenance point, housekeeping service, funeral service, lottery sales point, pet service, newsstand, public toilet, beauty, hairdressing, manicure, body beauty, resorts, farmyard, cinema, KTV, theater, dance hall, internet cafe, gaming venue, bathing massage, leisure plaza, sports venue, extreme sports venue, fitness center, car sale, car repair, car beauty, auto part, car rental, car inspection field, bank, ATM, credit union, investment and wealth management, pawnshop, office building
Industrial	Company, park, agriculture, forestry, horticulture, factory, and mine
Institutional	Institution of higher learning, middle school, primary school, kindergarten, adult education, parent-child education, special education school, intermediary, research institution, training institution, library, science and technology museum, Press and publication, radio and television, art group, art gallery, exhibition hall, cultural palace, General hospital, specialist hospital, clinic, pharmacy, medical examination institution, nursing home, emergency center, disease control center, central institution, governments at all level, administrative unit, public security agencies, foreign-related institution, party organization, welfare agency, political and educational institution
Recreational	Park, zoo, botanical garden, amusement park, museum, aquarium, bathing beache, heritage site, church, scenic area, island, mountain, water system
Transport	Airport, railway station, subway station, subway line, long-distance bus station, bus station, bus line, port, parking lot, refueling station, service area, toll station, bridge, charging station, roadside parking space, highway exit, highway entrance, airport exit, airport entrance, station exit, station entrance, parking lot entrance and exit

Source: Authors' classification based on Baidu Map.

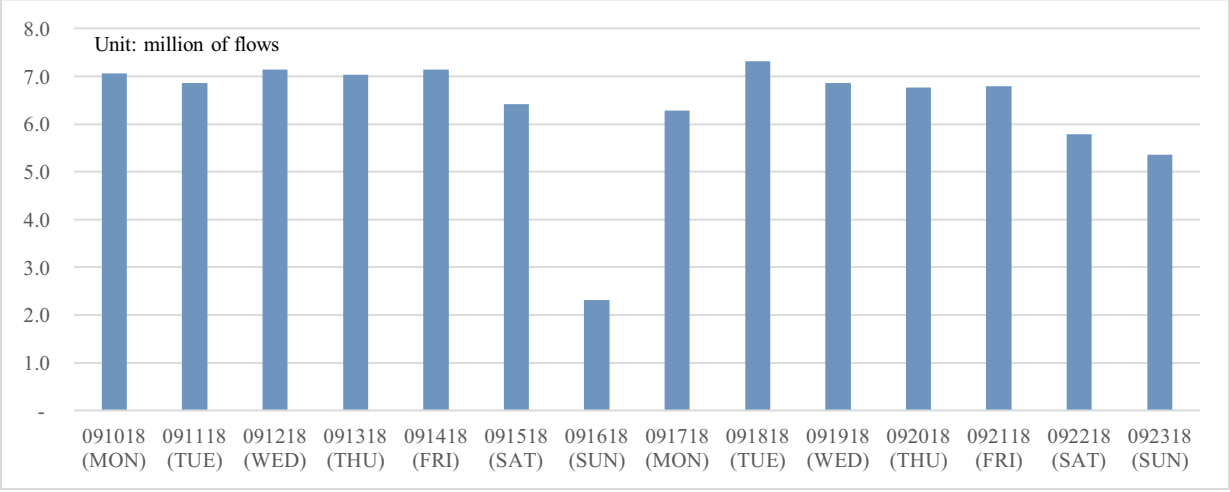

Fig. 1. Temporal distribution of flow volume during the investigation period.

better visualization of the major urban flows within the city, all flows with a value greater than “50” are presented in Fig. 2(d). It is evident that while some long distance trips are sporadically scattered with linkages between the east and the west, most of the flows have relatively short trip distances. Again, these activities are primarily concentrated in central and western districts where the level of human activities is generally high.

4. Methodology

4.1. Analytical framework

The analytical framework of spatiotemporal and functional flow pattern extraction is illustrated in Fig. 3. To begin with, the POI data and flow data were processed and cleaned by removing any abnormal records, such as outliers. The cleaned data were then adopted for both GIS analysis and spatial flow analysis. Specifically, various spatial maps were generated based on the cleaned data in order to provide a visualization of the spatial distribution of urban functions and flow activities. Next, the POI data were integrated with the flow data, based on the classification of land use type of the origin and destination of each flow. Meanwhile, global flow patterns of spatial association and local flow clustering were examined and compared over time. In the end, the identified functional and spatial patterns of the flow data were combined to assess the influence of the typhoon.

4.2. Functional flow distribution

To examine to what extent urban flows vary by urban function, the land use information of origin and destination and flow information were connected. Specifically, following previous studies such as Hu et al. (2016), Liu et al. (2017), Zhang et al. (2017), and Yang et al. (2019), the data was processed based on the following assumptions. First, we assume that the function of urban flow can be classified based on the land use type of the parcel of its origin and destination (OD). Second, POI data is assumed to be more relevant than the land use zoning data to reveal urban vitality given that the information tends to be updated more frequently than the traditional land use data. According to the standards of *land use, urban land classification, planning, and construction, urban functions*, urban function is reclassified into 6 essential categories based on information from the secondary classification of POIs from Baidu Maps: residential, commercial, industrial, institutional, recreational, and transport. Third, although POI data can be updated frequently, our assessment was conducted based on the assumption that the information of POI didn't change during the time period of this study.

Next, the POI data was aggregated at a block level. The block is defined by the same grid of 500 m × 500 m cells that the flow data use.

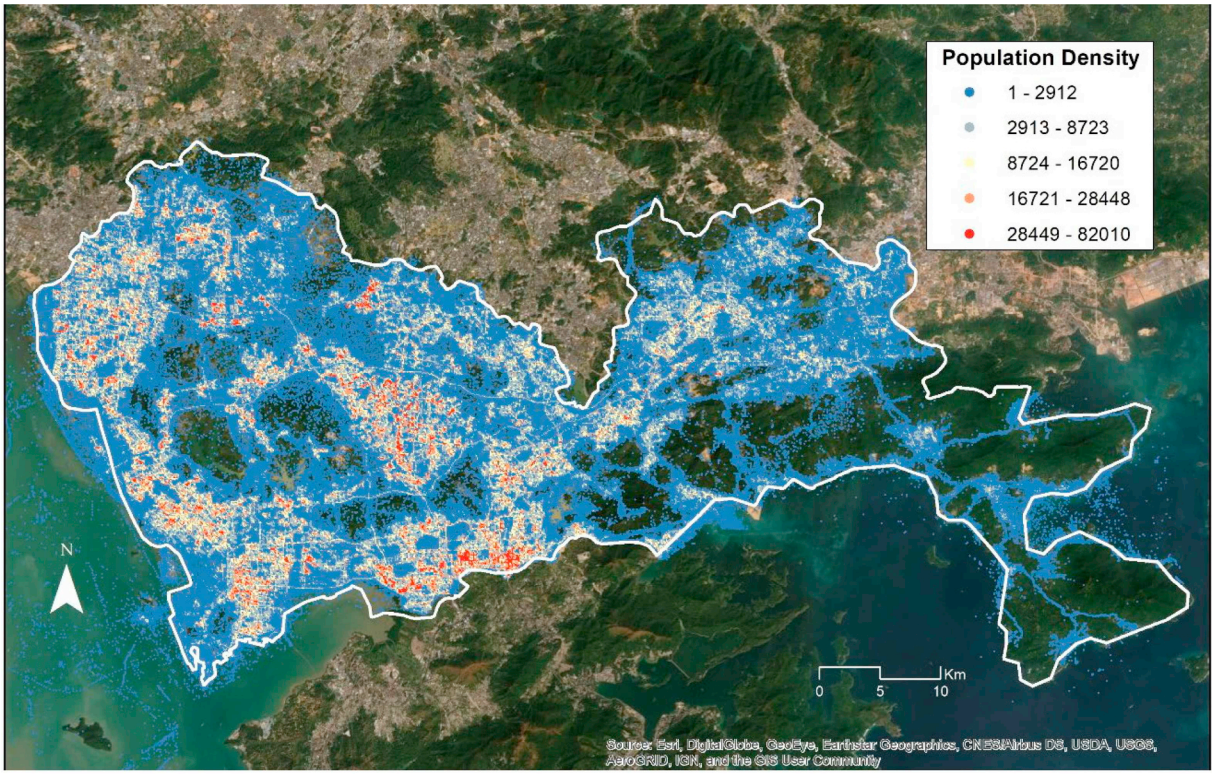

(a) Heat Map

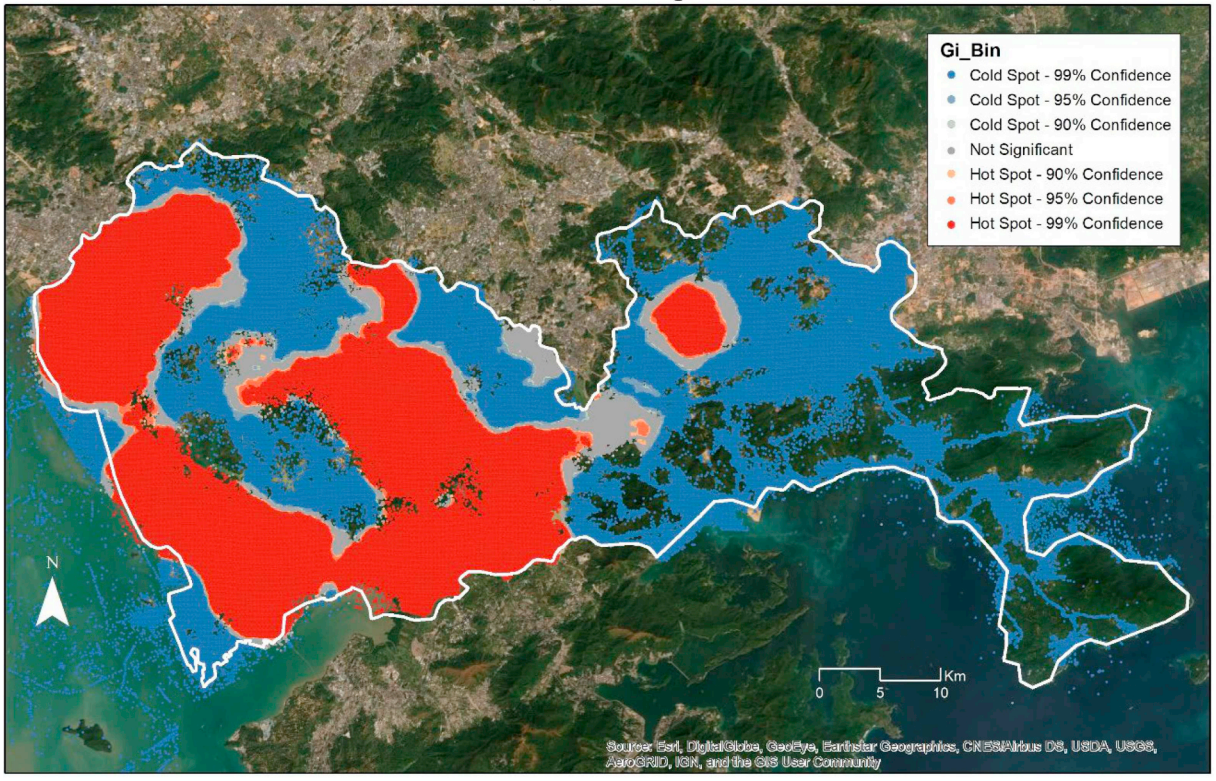

(b) Hotspot Map

Fig. 2. Spatial distributions of the LBS data in shenzhen.

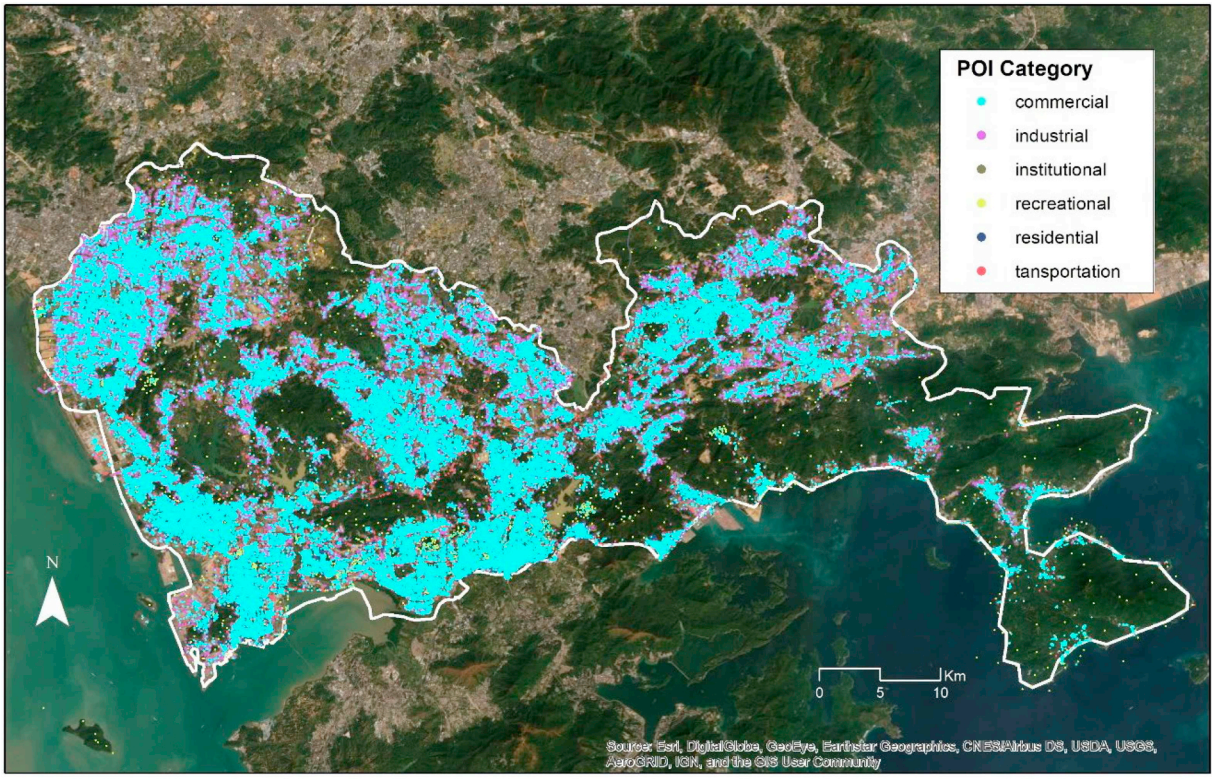

(c) Distribution of Urban Functions (based on POI)

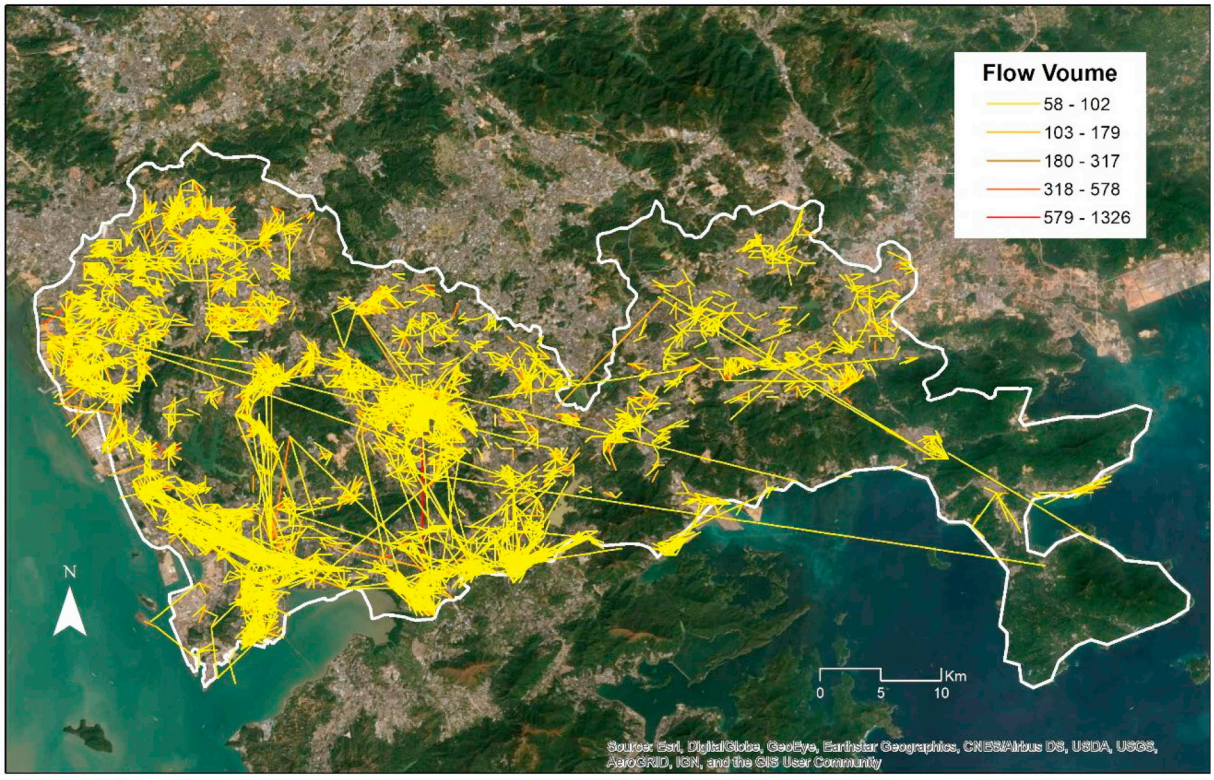

(d) Urban Flow (Only the flow value >50 were displayed)

Fig. 2. (*continued*)

The major urban function of each block is defined by the land function type with the highest share in each block. For instance, assuming S_n represents the aggregate number of POIs of the n category of land function in a certain block. The land function with the largest number of POIs is defined as $S_{high} = \max_{n\in[1,2,\ldots,6]} S_n$. Hence, the urban function can be defined by the land function with the highest percent of POIs (P_{high}),

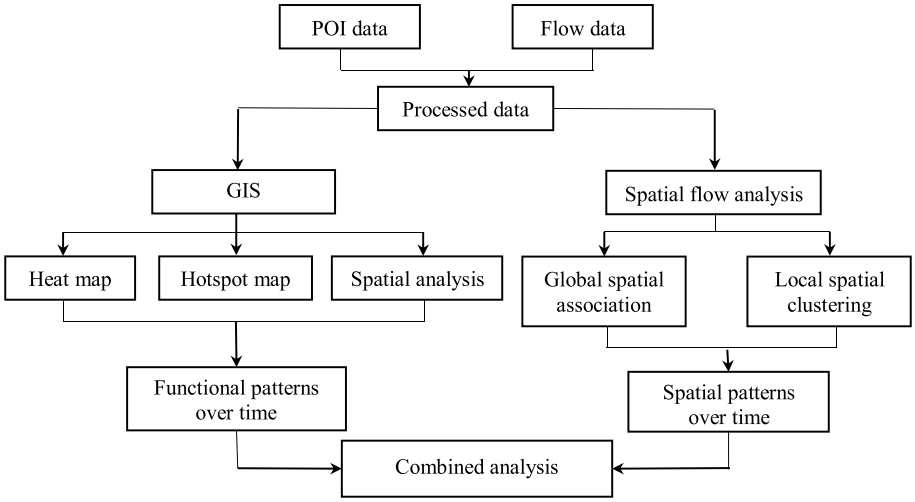

Fig. 3. A framework of spatiotemporal and functional flow pattern extraction.

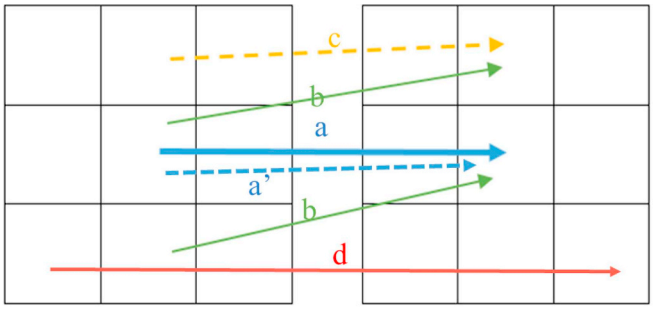

Fig. 4. Different cases of flow neighbor relationship.

which can be calculated through the following equation:

$$P_{high} = \frac{S_{high}}{\sum_{i=1}^{6} S_n} \times 100\% \quad (1)$$

One should note that there are several caveats of such a calculation. Firstly, the calculation is based on the quantity of POIs instead of the actual size of land uses. Secondly, the major urban function of each block is essentially determined by the function of land with the highest rate, which may not be realistically appropriate in a case where the shares of more than two types of land are equal.[2] Nevertheless, such a calculation provides a straightforward approach to identify the major function of each block.

Then, the urban flow with information of urban function was developed by joining each spatial flow with its corresponding major urban functions of its origin and destination blocks, respectively. In the end, a matrix that summarizes functional flows by type was generated to represent the functional distribution of flows.

4.3. Spatiotemporal flow pattern extraction

4.3.1. Global flow pattern of spatial association

The global flow pattern of spatial association needs to be extracted for each day of the entire period, which enables a longitudinal comparison of global spatial patterns of flow on a daily basis. To examine the global flow patterns of spatial association, the Getis-Ord General G statistic was adopted (Getis and Ord, 1992). This General G statistic is given by Eq. 2.

$$G = \frac{\sum_{i=1}^{n}\sum_{j=1}^{n} w_{ij}x_i x_j}{\sum_{i=1}^{n}\sum_{j=1}^{n} x_i x_j}, \forall\ i \neq j \quad (2)$$

where x_i represents the flow value of a flow i; w_{ij} is the spatial weight between flows i and j representing the spatial proximity between them. This statistic measures the global concentration of high or low flow values in the study area via the output G value and the associated Z-score and p-value.

To accommodate this classic statistic of high/low value clustering designed for point and areal data in the context of flow data, a formal definition of proximity for flows are crucial. We employ the neighborhood definition for flow data in Tao and Thill (2018). For a target flow A, its neighbors are defined according to following rules:

- Rule 1: Flows have the same origin and same destination as *a*;
- Rule 2: Flows have the same origin (destination) as a but a destination (origin) as the contiguous neighbor of *a*'s destination (origin);
- Rule 3: Flows have both origin and destination as the contiguous neighbors of *a*'s origin and destination;
- Rule 4: Flows have the origin and destination different from those of *a* and they are also not the contiguous neighbors of *a*'s origin and destination.

As demonstrated in Fig. 4, flow a' shares the same origin and destination with flow a (Rule 1). The flow labelled as b (b') shares the same origin (destination) with flow a, and has a contiguous destination (origin) with destination of flow a (Rule 2). The flow c has both origin and destination contiguous to those of flow a (Rule 3). Neither the origin nor destination of flow d is the same or contiguous to flow a (Rule 4). Therefore, flow a' should be aggregated with flow a (Rule 1); flow b and flow c are considered neighbors of flow a (Rules 2 and 3), while flow d is not (Rule 4).

4.3.2. Local flow clustering

The global flow pattern of spatial association cannot exhibit spatial clustering of flows at the local level due to the existence of spatial heterogeneity (Anselin, 1995). It necessitates detecting the spatial concentration of flows with similar flow values at the local level, namely hot or cold spots of flows. To extract the local flow pattern for each day of the period, a robust flow clustering method, flowAMOEBA (Tao and Thill, 2018), was adopted. FlowAMOEBA is a data-driven and bottom-up spatial statistic method for identifying spatial flow clusters

[2] There are two possibilities to address such a limitation. The first approach is to validate and update the outcomes based on other data sources, such as the land use data. The second approach is to improve the calculation formula by introducing a weight factor, such as area size of the facilities.

of high or low-value flows with irregular shapes, for the grouping of origin and destination locations. The method extends the classical spatial clustering method AMOEBA (Aldstadt and Getis, 2006) to allow areal data to work with flow data by properly defining spatial flow neighborhoods, as previously described.

To identify flow clusters, the algorithm starts from an arbitrary seed flow and attempts to iteratively expand the cluster towards neighboring flows with the aim of maximizing or minimizing the local G_i^*statistic (Getis and Ord, 1992; Ord and Getis, 1995), defined as follows:

$$G_i^* = \left(\sum_{j=1}^{N} w_{ij}x_j - \bar{x}\sum_{j1}^{N} w_{ij}\right)/S\sqrt{\frac{N\sum_{j=1}^{N} w_{ij}^2 - \sum_{j1}^{N} w_{ij}^2}{N-1}}, \text{ where } S = \sqrt{\frac{\sum_{j=1}^{N} x_j^2}{N} - \bar{x}^2} \quad (3)$$

In this study, we set the spatial weight w_{ij} equal to 1 if flow j neighbors flow i, and 0 otherwise. N is the total number of flows, x_j is the value of flow j, and $\bar{x}$ is the mean value of all flows. With the identified flow clusters from all predetermined seeds, they are sorted by their absolute G_i^* values. The ones with the highest values without any spatial overlaps were preserved. Finally, Monte-Carlo simulations were carried out to select the flow clusters that pass statistical significance tests as the final results.

Once the local flow clustering patterns were extracted for every day, how to compare the clustering patterns on a daily basis became a challenge. As the local flow clustering patterns for each day are represented by a set of flow clusters, with each cluster including a number of flows, it is a nontrivial task to compare the structures of two or more clustering patterns. Although simple statistics of each flow clustering pattern can be generated for a preliminary comparison, such as the number of clusters, min/max flow volume for single flow clusters, and total and mean flow volume for all clusters, there is a lack of measures that compare the spatial distribution of flow clusters for clustering patterns. All existing measures of clustering comparison assume the same set of data, based on which two clustering patterns are compared (Meilă, 2007). However, local flow clustering patterns extracted for different days in our study are from different data sets. Specifically, denote $f_{i,j}{}^d$ as the flow from location i to j for the date d ($i, j \in L$; d$\in D$; L is the set of locations in the study area and D is the set of dates for the period in this study) and F^d is the set of flows for date d. Then, we have:

$$f_{i,j}^d = \begin{cases} 1, \textit{ if } f_{i,j}^d \in F^d \\ 0, \textit{ otherwise} \end{cases} \quad (4)$$

After applying flowAMOEBA to F^d, a set of local flow clusters $P^d \subset F^d$ was extracted, where P^d is a subset of F^d. Therefore, for two flow patterns P^A and P^B for two dates respectively, they may include the same or different set of flows, which could violate the above assumption of existing measures. To remedy this issue, a Global Preservation Ratio (GPR) was for the first time developed to measure the general similarity of two patterns following the idea of the Jaccard index (Ben-Hur et al., 2001), which is known as the Intersection over Union of two sets of flows.

$$GPR = \frac{|P^A \cap P^B|}{|P^A \cup P^B|} \quad (5)$$

where $|* \mid = \Sigma_i\Sigma_j f_{i,j}{}^d, f_{i,j}{}^d \in *$, $*$ is a set of flows. Then, the similarity of the two patterns needed to be further examined at the individual cluster level, but only within the intersection set of the two patterns $I^{AB} = P^A \cap P^B$. Hence, given P^A and P^B, the intersection set I^{AB} can be represented as two partitions, namely $\{p_1, p_2, \ldots, p_k, \ldots\}$ based on P^A and $\{q_1, q_2, \ldots, q_l, \ldots\}$ based on P^B, respectively. Inspired by the Variation of Information (VI) measure (Meilă, 2007), a Local Preservation Ratio can be defined as:

Table 3
General G statistics for global flow pattern of spatial association.

Date	G value	P-value	Z-value
Sep-10-2018	0.000359	0.459028	0.103
Sep-11-2018	0.000513	0*	17.360
Sep-12-2018	0.00035	0.477715	0.056
Sep-13-2018	0.000392	0.375192	0.318
Sep-14-2018	0.000358	0.457267	0.107
Sep-15-2018	0.000351	0.474665	0.064
Sep-16-2018	0.000187	0.456697	−0.109
Sep-17-2018	0.000349	0.463495	0.092
Sep-18-2018	0.000273	0.46399	−0.090
Sep-19-2018	0.000471	5.67E-05*	3.860
Sep-20-2018	0.000535	0*	61.108
Sep-21-2018	0.000525	0*	61.982
Sep-22-2018	0.000555	0*	58.015
Sep-23-2018	0.000465	0*	37.806

* 99% significance level.

$$LPR = \sum_k \sum_l \frac{|p_k \cap q_l|}{|I^{AB}|}\frac{|p_k \cap q_l|}{|p_k \cup q_l|} \quad (6)$$

where the first item $\frac{|p_k \cap q_l|}{|I^{AB}|}$ serves as a local weight reflecting the density of the overlap between two clusters from different partitions, while the second item $\frac{|p_k \cap q_l|}{|p_k \cup q_l|}$ is a local version of the Jaccard index. Similar to VI, LPR is weighted by the local density of the overlap between any two clusters from different partitions, representing the importance of the similarity of two clusters at the local level. Unlike VI, which uses an information-entropy-based distance measure as the second item, LPR measures the local similarity based on the set theory which is consistent with that of GPR. Furthermore, it allows the values of GPR and LPR to be more straightforward and interpretable, as they are naturally bounded between 0 and 1. However, VI needs to be normalized to achieve this. Consequently, it enables the combination of the GPR and LPR as a Total Preservation Ratio (TPR), which can be formulated as:

$$TPR = GPR \bullet LPR \quad (7)$$

5. Results

5.1. Spatial-temporal flow patterns

Table 3 shows the General G statistic as an indicator of the global flow pattern of spatial association for each day in the study period. It indicates that only six days (11th, 19th, 20th, 21st, 22nd, and 23rd of September) exhibited a significant global spatial concentration of high-volume human mobility flows. For the rest of the dates, the spatial distribution of human mobility flows seemed to follow a random pattern. For the day of disruption (16th), it does not show a distinct pattern from those of the adjacent days.

As discussed before, indicators for the global pattern of spatial association cannot reflect spatial clustering at the local level. FlowAMOEBA is applied to extract local clusters of high-volume flows for each day in the study period. The same method settings are used for consistency, such as the significance level (99%) and number of permutations (1000). Fig. 5 displays daily variations of local flow clusters generated from the analysis. The visualization of flow clusters provides a straightforward approach to understanding the spatial distribution of urban flow clusters and its evolution over time. The comparison of daily flow clusters reveals that the flow clusters of human mobility on September 16th did exhibit distinct characteristics from other days, as both the number of clusters and the flow volume were reduced significantly due to the disruption from Typhoon Mangkhut.

To further compare the spatial distribution of local flow clusters on different days, Preservation Ratios were computed for the local flow patterns of two consecutive days (Fig. 6) to reflect the temporal

Fig. 5. Daily variation of local flow clustering (Sep 10–23, 2018).

changes. Two disruptions are identified in Fig. 6. The first is around the 15th and 16th, where low values of all three preservation ratios indicate a dissimilarity in patterns between the 15th and 16th and the 16th and 17th. In other words, the spatial distribution and clustering of human mobility flows on 16th is significantly different from those for the day before (15th) and the day after (17th). This can reflect a process of normal-disruption-recovery that occurred during the three consecutive days. It should be noted that among the common flows (GPR) identified in the flow clustering between two consecutive days, the local spatial clustering pattern (LPR) is less different between 15th and 16th than the 16th and 17th. This can be attributed to the fact that the 15th and 16th were the weekend and share more commonalities in term of human mobility than with 17th (Monday).

The second identified disruption was on the 20th, shown by the low preservation ratios between the 19th and 20th. Unlike the first disruption, the local spatial flow pattern for the 20th is similar to that for the 21st, which means there is not a recovery on the day after the disruption. This disruption is unexpected, as it is just three days after the recovery from the disruption on the 16th. To further examine the validity and cause of this disruption, a pairwise comparison between the local flow patterns of each day was conducted and the results are presented in the form of a similarity matrix plot (Fig. 7). First, the disruption on the 16th caused by Typhoon Mangkhut is confirmed. The comparison between GPR and LPR indicates that the dissimilarity lies more in the unshared flows than the grouping of the shared set of flows into clusters. In other words, the disruption from the storm caused many flows to disappear. Secondly, the disruption that began on the 20th was also confirmed and this disruption continued for the rest of the study period. It is evidenced by the inter-group pattern differences between flow patterns for the sub-period of the 20th – 23rd and those

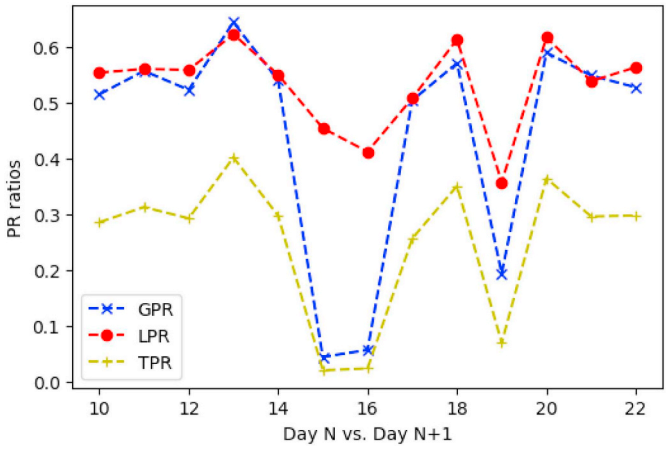

Fig. 6. Variation of the preservation ratios, GPR, LPR, and TPR, over time.

for the sub-period of the 10th – 19th (excluding the 16th), and by the relatively high similarity between flow patterns within each sub-period. The fairly high similarity between patterns from the 20th – 23rd is also reflected by the General G statistics in Table 3, which are more similar to days within this sub-period rather than the days outside of it. Experientially, this disruption could be attributed to the fact that the Mid-Autumn Festival was on the 24th, which is one of the most important national holidays for family reunions. To make sure they are able to return to their hometown on that day, people in China usually begin their travels several days earlier, which collectively leads to a large number of human mobility flows towards transportation stations, hubs, and ports, thus leading to distinctly different flow patterns from normal days.

5.2. Functional flow patterns

Table 4 provides a summary of the flow change by urban function during Typhoon Mangkhut based on the entire observations of flow. Specifically, Table 4(a) summarizes the percent change of urban flow from one type of urban function to another one on the first day (Sep 16, 2018). The percent change was calculated by comparing the corresponding day of a week either before or after the typhoon event. It is clear that the occurrence of Typhoon Mangkhut had a substantial impact on urban flow in Shenzhen, as volume was reduced by an average of 60.8% on the first day of the storm. The most affected functions include commercial, recreational, and transport-related flows. Conversely, the flows with either an institutional or industrial-related origin/destination were found to have a relatively lower average reduction on the first day of the event.

Table 4(b) summarizes the change in urban flow by function in the second day of the typhoon event. It is evident that the level of disruption on the second day is much lower than the first day, as only 11.1% of the flows were reduced. Similarly, flows that either originated or ended at recreational areas such as parks, museums, and scenic sites were found to have experienced relatively higher decreases than other function categories. Conversely, flows that involve a function such as institutional and residential were found to have a much lower decrease. Such results confirm that during extreme weather or disaster events, flows related to fundamental urban functions such as businesses, manufacturing, education, hospitals, and media agencies tend to experience a relatively lower level of disruption, whereas flows that involve leisure and recreational functions are more likely to experience a

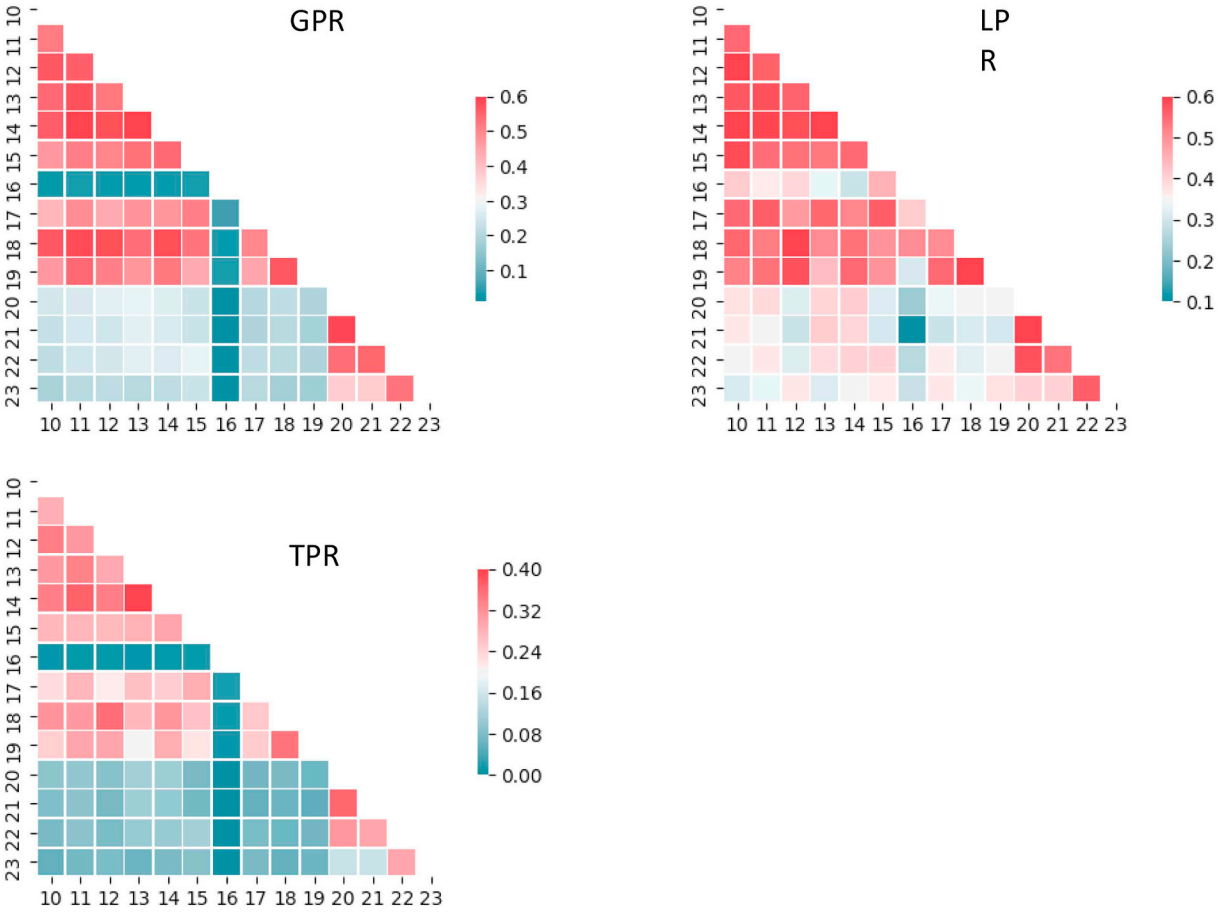

Fig. 7. Correlation matrix of daily spatial cluster patterns based on preservation ratios.

Table 4
Urban flow change by function during the typhoon event. (Comparison with the corresponding weekday.)

(a) The first day of the typhoon event (Sep 16, 2018)

		Destination						
	Type	Commercial	Industrial	Institutional	Recreational	Residential	Transport	Total
Origin	Commercial	−64.0%	−59.2%	−63.0%	−70.8%	−64.9%	−67.4%	−63.3%
	Industrial	−59.5%	−49.5%	−43.2%	−50.8%	−57.7%	−53.9%	−55.6%
	Institutional	−63.9%	−42.9%	−48.0%	−67.1%	−57.8%	−59.2%	−57.2%
	Recreational	−70.9%	−51.8%	−64.3%	−69.6%	−67.0%	−64.0%	−64.2%
	Residential	−64.0%	−56.9%	−57.9%	−64.0%	−56.3%	−61.3%	−61.3%
	Transport	−65.5%	−52.8%	−58.8%	−62.2%	−60.4%	−55.9%	−60.8%
	Total	−63.1%	−55.3%	−56.7%	−63.5%	−61.9%	−62.2%	−60.8%

1. The calculation is based on: (Flowsep.16 – Flowsep.23)/ Flowsep.23 × 100%
2. The summary was calculated based on the 89 million of flow samples.
3. Exclude other types of urban functions.

(b) The second day of the typhoon event (Sep 17, 2018)

		Destination						
	Type	Commercial	Industrial	Institutional	Recreational	Residential	Transport	Total
Origin	Commercial	−10.0%	−9.1%	−12.1%	−17.0%	−9.7%	−11.2%	−10.1%
	Industrial	−11.0%	−8.3%	−10.8%	−10.5%	−9.5%	−13.1%	−10.4%
	Institutional	−15.7%	−13.0%	−12.8%	−25.5%	−13.8%	−14.9%	−15.0%
	Recreational	−20.5%	−13.9%	−26.1%	−23.0%	−23.6%	−15.6%	−19.3%
	Residential	−10.4%	−8.2%	−10.6%	−21.6%	−6.3%	−7.0%	−9.7%
	Transport	−14.9%	−13.7%	−16.1%	−17.4%	−11.2%	−15.0%	−14.8%
	Total	−11.1%	−9.5%	−12.8%	−16.8%	−10.1%	−12.4%	−11.1%

1. The calculation is based on:(Flowsep.17 – Flowsep.10)/ Flowsep.10 × 100%
2. The summary was calculated based on the 89 million of flow samples.
3. Exclude other types of urban functions.

Table 5
Urban flow change by function during and after the typhoon event. (The comparison is based on the average level.)

(a) The average flow during the event (Sep. 16–17, 2018)/The average daily flow before the event (Sep. 10–15, 2018)

		Destination						
	Type	Commercial	Industrial	Institutional	Recreational	Residential	Transport	Total
Origin	Commercial	−40%	−38%	−41%	−44%	−39%	−43%	−40%
	Industrial	−40%	−35%	−34%	−33%	−37%	−39%	−38%
	Institutional	−44%	−36%	−37%	−44%	−40%	−41%	−41%
	Recreational	−46%	−36%	−44%	−37%	−43%	−42%	−43%
	Residential	−39%	−36%	−38%	−41%	−34%	−38%	−38%
	Transport	−44%	−39%	−42%	−42%	−40%	−41%	−42%
	Total	−40%	−37%	−39%	−40%	−38%	−41%	−39%

1. The calculation is based on (The average flow of Sep 16–17 – The average flow of Sep 10–15)/The average flow of Sep 10–15 × 100%.
2. The summary was calculated based on the 89 million of flow samples.
3. Exclude other types of urban functions.

(b) The average flow after the event (Sep. 18–23, 2018) /
The average daily flow during the event (Sep. 16–17, 2018)

		Destination						
	Type	Commercial	Industrial	Institutional	Recreational	Residential	Transport	Total
Origin	Commercial	58%	53%	60%	71%	58%	63%	57%
	Industrial	56%	46%	39%	45%	51%	53%	52%
	Institutional	67%	43%	47%	82%	59%	56%	58%
	Recreational	78%	49%	78%	70%	68%	66%	67%
	Residential	58%	49%	53%	59%	49%	54%	55%
	Transport	67%	53%	59%	65%	58%	55%	61%
	Total	59%	51%	54%	62%	56%	59%	56%

1. The calculation is based on (The average flow of Sep 18–23 – The average flow of Sep 16–17) / The average flow of Sep 16–17 × 100%.
2. The summary was calculated based on the 89 million of flow samples.
3. Exclude other types of urban functions.

higher disruption level.

To test the consistency of the research findings, Table 5 summarizes urban flow change by function based on a comparison of the average flow volume before, during, and after the typhoon based on a different formula. Specifically, the change in flow by function presented in Table 5(a) was calculated based on the difference of the average flow volume change between the period of "during the typhoon" (September 16–17) and "before the typhoon" (September 10–15). This calculation has the advantage of smoothing out the temporal variation caused by different days of the week. Hence, the pattern is likely to be more reliable and consistent than the pattern revealed in the daily flow comparison. The overall impact of Typhoon Mangkhut on urban human flows was found to be 39%, suggesting that during the two days the storm was present, approximately 39% of urban flows in Shenzhen were reduced.

In terms of the comparison by function of flow, the results were found to be more consistent among different categories of functions. For instance, the flows with destinations at commerce and recreation-related locations, such as restaurants, hotels, shopping centers, and parks, generally experienced a reduction in average flow volume by 40%, whereas the reduction was relatively lesser for fundamental functions such as industry and residential.

Table 5(b) calculates the recovery of urban human flows by various functions after the typhoon event. The calculation was conducted using differences in the average flow during and after the duration of the storm. In general, the results show that 56% of urban flows were recovered during the period immediately after the typhoon's departure. Again, leisure and recreation-related flows experienced the highest level of change. The flows related to commercial and transportation purposes also experienced a relatively high level of recovery (given that 59% of flows were recovered after the disruptive event). Conversely, the categories of flow with fundamental functions, such as business and residence experienced a relatively low magnitude of change.

5.3. Functional patterns of flow clusters

The variations in urban flow by different functions was also examined with a focus on major clusters. These clusters were identified using the FlowAMOEBA method. In total, the identified clusters account for 4.4% of the total observed flows. One should note that the understanding of the spatial-temporal variation of flow clusters have important implications, given that flow clusters generally represent spatial distributional patterns of major urban human activities. If we assume the regions or areas with the highest volume of urban flows would deserve more attention under disruptive events, the analysis outlined in this study would be helpful to identify those locations easily and thus provide with more targeted guidance for emergency response and management. Following a similar approach, the change in flow clusters by different functions was calculated based on the various days of the typhoon. As shown in Tables 6 (a) and 6(b), around 90% of the flow clusters were reduced on the first day of the event as compared with the corresponding day in a normal circumstance, whereas only 19% of the flow clusters were reduced on the second day of the event. Although most flow clusters by different functions experience a negative change, one should note that counterintuitive outcomes, such as a positive change in certain flow clusters during the storm, were also observed. This may be partially due to the relatively small number of observations in the case of cluster calculation. Such an outcome may also be due to the specific pattern of the selected reference day.

6. Discussion and conclusions

In the era of smart cities, the massive adoption of sensor-based ICT technology and open LBS platforms have generated a large volume and variety of spatial data at an unprecedented rapid pace. These data provide urban planners and analysts with new sources to better understand challenging issues pertaining to resilience and sustainability. This study evaluates the impact of extreme weather events on urban human flow using location-based big data from Baidu Map. Using

Table 6
Urban flow change by function of clusters. (Comparison with the corresponding weekday.)

(a) The first day of the typhoon event (Sep 16, 2018)

	Destination						
	Type	Commercial	Industrial	Institutional	Recreational	Residential	Transport	Total
Origin	Commercial	−94%	−91%	−100%	−100%	−99%	−88%	−93%
	Industrial	−92%	−90%	384%	98%	−93%	−45%	−85%
	Institutional	−100%	101%				−100%	−47%
	Recreational	−100%	143%					13%
	Residential	−99%	−98%			−100%	−100%	−99%
	Transport	−87%	−68%	−100%		−100%	−100%	−84%
	Total	−94%	−87%	60%	−10%	−98%	−83%	−90%

1. The calculation is based on: (Flow sep.16 – Flowsep.23)/ Flowsep.23 × 100%.
2. The summary was calculated based on the flow clusters.
3. Exclude other types of urban functions.

(b) The second day of the typhoon event (Sep 17, 2018)

	Destination						
	Type	Commercial	Industrial	Institutional	Recreational	Residential	Transport	Total
Origin	Commercial	−5%	−15%	−91%	−83%	0%	−22%	−11%
	Industrial	−21%	−26%	−11%	−26%	−19%	−34%	−25%
	Institutional	−79%	−43%					−56%
	Recreational	−42%	−24%			−100%		−49%
	Residential	−30%	−26%	−100%	−100%	405%	2%	−26%
	Transport	−39%	−46%			−1%	−7%	−36%
	Total	−15%	−23%	−51%	−57%	−10%	−23%	−19%

1. The calculation is based on: (Flowsep.17 – Flowsep.10)/ Flowsep.10 × 100%.
2. The summary was calculated based on the flow clusters.
3. Exclude other types of urban functions.

Typhoon Mangkhut as an example, the spatiotemporal and functional variations of urban human flow in Shenzhen are examined using various methods, including GIS and spatial flow analysis methods. To our limited knowledge, this is the first application using both flow data and POI data to examine the impact of extreme weather events on human flow changes, with a comparison of various urban functions.

The study revealed that urban flows have been impacted substantially not only in volume but also in terms of their spatial and functional patterns during the typhoon event. In terms of the temporal variation, our analysis reveals that urban flows were found to have reduced by 39% during the disruption. Conversely, 56% of flows increased immediately after the disruption. In terms of spatial pattern, the disruptive weather event has caused a significant change of local spatial clustering of mobility flows. In addition, one noteworthy pattern after the landfall of the typhoon was also identified. During September 20 and 23, spatial flow patterns of both global spatial association and local spatial clustering are found to be dramatically different from that of other days, which suggests that there could be a different event rather than underlying Typhoon Mangkhut. As discussed earlier, in this case, the pattern may reflect a different pattern of mobility which may be caused by the increased amount of family reunion trips for the Mid-Autumn Festival (Sep 24). In short, our analysis provides a novel approach to evaluate the impacts of various disruptions on urban mobility through coupling flow clustering methods (e.g., FlowAMOEBA) with the new developed measure of pattern comparison. Such an approach enables us to effectively quantify the dynamic change of spatial clustering patterns of urban mobility and other flow-based geographic phenomena, which was lacking in the existing GIS toolboxes.

In terms of functional variation, the assessment revealed that fundamental urban functions such as industrial (work) and institutional (education) related trips experienced less disruption, whereas recreational related trips tend to receive a relatively larger influence by the typhoon event. Overall, the research findings confirm that there is a strong connection between urban flow and urban function. The result is consistent with previous studies in terms of the relationship between urban flow and urban functions (Calabrese et al., 2010; Lee and Holme, 2015; Pan et al., 2012; Yang et al., 2019; Yuan et al., 2012; Zhang et al., 2017). One should note that most of these previous studies attempted to reveal the linkage of human mobility with urban function in normal conditions.

Our study, on the contrary, extends the assessment from the literature with a focus on examining the variations of human mobility in different urban functions under abnormal condition. We believe such an extension is important as it would help us recognize to what extent the urban flow is disrupted due to unexpected events, which hence may provide important implications for planners and policy makers to enhance urban disaster resilience through a better understanding of urban vulnerability to various types of unexpected events, such as extreme weather events and contagious disease outbreaks.

For instance, the LBS data and method developed in this study can be used to evaluate the effectiveness of flow mobility by different urban functions under a disruptive event, such as typhoon and flood event. The outcome of these assessments would provide evidence and support to allocate resources to restrict human activities and guarantee the safety of human mobility. In addition, the analysis will also have a potential to be applied for the evaluation and a temporary restriction of flow movement in the case of human pandemic, such as the recent outbreak of the 2019 novel coronavirus occurred in China. With the capability of LBS data and analytical framework developed in this study, human urban flow could be adopted as a GIS visualization system to assist first responders to achieve dynamic monitoring, tracking and assessing the human flow capacity of the urban infrastructure systems. This may eventually facilitate the development of more targeted emergency planning strategies that will enhance urban resilience to various types of unexpected events in the future.

One should note that our study also has several limitations. First, the research outcomes can be sensitive to the data used. For instance, the different results found through the comparison of the functional patterns of flow clusters to the total population suggest that it would be better to adopt a more representative LBS data, in order to reveal a more reliable calculation outcome in future analyses. In addition, the POI data used in this study is mainly pertinent to commercial activities and lacks adequate points for activities such as recreation, which may cause bias when classifying land functions, regardless of the fact that POI data is able to reflect the vitality of a city. Furthermore, a lack of assigned weights on POI data could lead to biased identification of the major urban functions in each block area. Hence, it would be worthwhile adopting different resources, such as both POIs and urban land use maps, in order to generate a more accurate representation of urban functions by different unit areas.

One should also note that the comparative framework could also be improved in several aspects in future research. For instance, the results would be more reliable if a longer-term data is adopted for a temporal comparison of flow changes. In addition, the accuracy of the analysis could be further improved if the data at hourly intervals could be utilized. This would help to separate the influences of other factors, such as weekly temporal effects or the effects of other special holiday events, which hence may provide more useful information for planning practice and emergency response.

Thirdly, although for a demonstration purpose, our assessment focuses on a single city of evaluation, the study could be also expanded to other cities and/or for different disruptive events. For instance, it would be interesting to compare to what extent the responses of urban flow vary among various cities with different urban spatial structure. Such an assessment could be further linked to economic impact analysis for an evaluation of the effectiveness of the existing urban spatial structure under both normal and abnormal situations. These multidimensional assessments would enable us to gain a more comprehensive understanding of both social and economic impacts of disruptive events as a result of interruptions of urban flow activities.

Author agreement

All the authors approved the final version of the manuscript to be submitted to *Computers, Environment and Urban Systems*.

Acknowledgements

An earlier version of this paper was presented at the 2019 International Symposium on Location-Based Big Data in Tokyo, Japan. The authors would like to thank the comments received from the participants. We also would like to thank the three anonymous reviewers for providing valuable feedback to improve this paper. In addition, we appreciate Dr. Ran Tao for kindly providing the code of flowAMOEBA. Views presented in this study do not represent any organizations and authors are responsible for any errors or mistakes.

References

Ahmouda, A., Hochmair, H. H., & Cvetojevic, S. (2019). Using twitter to analyze the effect of hurricanes on human mobility patterns. *Urban Sci, 3*(3), 87.

Aldstadt, J., & Getis, A. (2006). Using AMOEBA to create a spatial weights matrix and identify spatial clusters. *Geographical Analysis, 38*(4), 327–343.

Anselin, L. (1995). Local indicators of spatial association—LISA. *Geographical Analysis, 27*(2), 93–115.

Bengtsson, L., Lu, X., Thorson, A., Garfield, R., & Von Schreeb, J. (2011). Improved response to disasters and outbreaks by tracking population movements with mobile phone network data: A post-earthquake geospatial study in Haiti. *PLoS Med, 8*(8), Article e1001083.

Ben-Hur, A., Elisseeff, A., & Guyon, I. (2001). A stability based method for discovering structure in clustered data. *In Biocomputing 2002,* 6–17.

Berke, P. R. (1995). Natural-hazard reduction and sustainable development: a global assessment. *Journal of Planning Literature, 9*(4), 370–382.

Brockmann, D., Hufnagel, L., & Geisel, T. (2006). The scaling laws of human travel. *Nature, 439*(7075), 462.

Calabrese, F., Di Lorenzo, G., & Ratti, C. (2010). Human mobility prediction based on individual and collective geographical preferences. *Paper presented at the 13th international IEEE conference on intelligent transportation systems*.
Chen, Z., & Schintler, L. A. (2015). Sensitivity of location-sharing services data: evidence from American travel pattern. *Transportation, 42*(4), 669–682.
Dewan, A. (2013). *Floods in a megacity: geospatial techniques in assessing hazards, risk and vulnerability*. Dordrecht: Springer119–156.
Getis, A., & Ord, J. (1992). The analysis of spatial association by use of distance statistics. *Geographical Analysis, 24*(3), 189–206.
Gonzalez, M. C., Hidalgo, C. A., & Barabasi, A.-L. (2008). Understanding individual human mobility patterns. *Nature, 453*(7196), 779.
Han, R. (2018). *Mangkhut wreaks havoc on SZ.* Shenzhen Daily. September 17 http://www.szdaily.com/content/2018-09/17/content_21086105.htm.
Han, S. Y., Tsou, M.-H., Knaap, E., Rey, S., & Cao, G. (2019). How do cities flow in an emergency? Tracing human mobility patterns during a natural disaster with big data and geospatial data science. *Urban Sci, 3*(2), 51.
Hu, T., Yang, J., Li, X., & Gong, P. (2016). Mapping urban land use by using landsat images and open social data. *Remote Sens (Basel), 8*(2), 151.
Joo, S., Kashiyama, T., Sekimoto, Y., & Seto, T. (2019). An analysis of factors influencing disaster mobility using location data from smartphones: Case study of Western Japan flooding. *J Disaster Res, 14*(6), 903–911.
Khaefi, M. R., Prahara, P. J., Rheza, M., Alkarisya, D., & Hodge, G. (2018). Predicting evacuation destinations due to a natural hazard using mobile network data. *Paper presented at the 2018 2nd international conference on informatics and computational sciences (ICICoS)*.
Lee, M., & Holme, P. (2015). Relating land use and human intra-city mobility. *PLoS One, 10*(10), Article e0140152.
Li, J. (2018). *Who will win the web mapping and navigation market in China, Baidu, Gaode, or Tencent?* SINA News. November 7 https://t.cj.sina.com.cn/articles/view/1456070103/56c9ddd701900et2c.
Liang, X., Zheng, X., Lv, W., Zhu, T., & Xu, K. (2012). The scaling of human mobility by taxis is exponential. *Physica A: Statistical Mechanics and its Applications, 391*(5), 2135–2144.
Liang, Y. (2018). Super typhoon Mangkhut lands on South China coast, Xinhua. September 16 http://www.xinhuanet.com/english/2018-09/16/c_137471874_2.htm.
Liu, X., He, J., Yao, Y., Zhang, J., Liang, H., Wang, H., & Hong, Y. (2017). Classifying urban land use by integrating remote sensing and social media data. *International Journal of Geographical Information Science, 31*(8), 1675–1696.
Liu, X., Derudder, B., & Wang, M. (2018). Polycentric urban development in China: A multi-scale analysis. *Environment and Planning B: Urban Analytics and City Science, 45*(5), 953–972.
Liu, Z., Du, Y., Yi, J., Liang, F., Ma, T., & Pei, T. (2019). Quantitative estimates of collective geo-tagged human activities in response to typhoon Hato using location-aware big data. *International Journal of Digital Earth,* 1–21.
Lu, X., Bengtsson, L., & Holme, P. (2012). Predictability of population displacement after the 2010 Haiti earthquake. *Proc Natl Acad Sci, 109*(29), 11576–11581.
Martín, Y., Li, Z., & Cutter, S. L. (2017). Leveraging twitter to gauge evacuation compliance: Spatiotemporal analysis of hurricane Matthew. *PLoS One, 12*(7), Article e0181701.
Meilă, M. (2007). Comparing clusterings—an information based distance. *Journal of multivariate analysis, 98*(5), 873–895.
Mileti, D. (1999). *Disasters by design: A reassessment of natural hazards in the United States.* Joseph Henry Press.
Oliveira, E. M. R., Viana, A. C., Sarraute, C., Brea, J., & Alvarez-Hamelin, I. (2016). On the regularity of human mobility. *Pervasive and Mobile Computing, 33*, 73–90.
Ord, J., & Getis, A. (1995). Local spatial autocorrelation statistics: Distributional issues and an application. *Geographical Analysis, 27*(4), 286–306.
Pan, G., Qi, G., Wu, Z., Zhang, D., & Li, S. (2012). Land-use classification using taxi GPS traces. *IEEE Transactions on Intelligent Transportation Systems, 14*(1), 113–123.
Papandrea, M., Jahromi, K. K., Zignani, M., Gaito, S., Giordano, S., & Rossi, G. P. (2016). On the properties of human mobility. *Computer Communications, 87*, 19–36.
Rhee, I., Shin, M., Hong, S., Lee, K., Kim, S. J., & Chong, S. (2011). On the levy-walk nature of human mobility. *IEEE/ACM transactions on networking (TON), 19*(3), 630–643.
Rose, A. (2004). Defining and measuring economic resilience to disasters. *Disaster Prevention and Management: An International Journal, 13*(4), 307–314.
Roy, K. C., Cebrian, M., & Hasan, S. (2019). Quantifying human mobility resilience to extreme events using geo-located social media data. *EPJ Data Science, 8*(1), 18.
Shaw, S. L., Tsou, M. H., & Ye, X. (2016). Human dynamics in the mobile and big data era. *International Journal of Geographical Information Science, 30*(9), 1687–1693.
Smith, A. B., & Katz, R. W. (2013). US billion-dollar weather and climate disasters: data sources, trends, accuracy and biases. *Natural hazards, 67*(2), 387–410.
Song, X., Zhang, Q., Sekimoto, Y., & Shibasaki, R. (2014, August). Prediction of human emergency behavior and their mobility following large-scale disaster. *Proceedings of the 20th ACM SIGKDD international conference on Knowledge discovery and data mining* (pp. 5–14). .
Tao, R., & Thill, J.-C. (2018). flowAMOEBA: Identifying regions of anomalous spatial interactions. *Geographical Analysis, 51*(1), 111–130.
Taylor, M. (2017). *Vulnerability analysis for transportation networks.* Elsevier.
Wang, Q., & Taylor, J. E. (2016). Patterns and limitations of urban human mobility resilience under the influence of multiple types of natural disaster. *PLoS One, 11*(1), Article e0147299.
Wang, Q., & Taylor, J. E. (2014). Quantifying, comparing human mobility perturbation during hurricane Sandy, typhoon Wipha, typhoon Haiyan. *Procedia Economics and Finance, 18*, 33–38.
Wang, Y., Wang, Q., & Taylor, J. E. (2017). Aggregated responses of human mobility to severe winter storms: An empirical study. *PLoS One, 12*(12), Article e0188734.
Xu, Z., Cui, G., Zhong, M., & Wang, X. (2019). Anomalous urban mobility pattern detection based on GPS trajectories and POI data. *ISPRS Int J Geo Inf, 8*(7), 308.
Yabe, T., & Ukkusuri, S. V. (2019a). Integrating information from heterogeneous networks on social media to predict post-disaster returning behavior. *Journal of Computational Science, 32*, 12–20.
Yabe, T., Sekimoto, Y., Tsubouchi, K., & Ikemoto, S. (2019b). Cross-comparative analysis of evacuation behavior after earthquakes using mobile phone data. *PLoS one, 14*(2), e0211375.
Yang, X., Fang, Z., Yin, L., Li, J., Lu, S., & Zhao, Z. (2019). Revealing the relationship of human convergence–divergence patterns and land use: A case study on Shenzhen City, China. *Cities, 95*, 102384.
Yuan, J., Zheng, Y., & Xie, X. (2012). Discovering regions of different functions in a city using human mobility and POIs. *Paper presented at the proceedings of the 18th ACM SIGKDD international conference on knowledge discovery and data mining*.
Zhang, T., Sun, L., Yao, L., & Rong, J. (2017). Impact analysis of land use on traffic congestion using real-time traffic and POI. *Journal of Advanced Transportation,* 2017.